Applied Magnetic Resonance (2020) 51:961–976
https://doi.org/10.1007/s00723-020-01262-6

Applied
Magnetic Resonance

ORIGINAL PAPER

Electron Spin Relaxation of Tb^{3+} and Tm^{3+} Ions

Joseph McPeak[1] · Dinu Alexander[2] · Cyriac Joseph[2] · Sandra S. Eaton[1] · Gareth R. Eaton[1]

Received: 17 July 2020 / Revised: 31 August 2020 / Published online: 14 September 2020

Abstract

Electron spin relaxation times T_1 and T_m of Tb^{3+} and Tm^{3+} in 1:1 water:ethanol and of Tb^{3+} doped (2%) in crystalline $La_2(oxalate)_3$ decahydrate were measured between about 4.2 and 10 K. Both cations are non-Kramers ions and have $J=6$ ground states. Echo-detected spectra are compared with CW spectra and with field-stepped direct-detected EPR spectra. Due to the strong temperature dependence of T_1, measurements were not made above 10 K. Between about 4.2 and 6 K T_1 is strongly concentration dependent between 1 and ~ 50 mM. T_1 values at 4.2 K are in the μs range which is orders of magnitude faster than for 3d transition metals. Phase memory times, T_m, are less than 500 ns, which is short relative to values observed for 3d transition metals and organic radicals at 4 K. T_m is longer in the oxalate lattice which is attributed to the lower proton concentration in oxalate than in the organic solvent, which decreases nuclear spin diffusion. The rigidity of the crystalline lattice also may contribute to longer T_m.

1 Introduction

Lanthanides are of on-going interest because of their wide range of optical and magnetic properties, possible applications in biomolecular structural studies, and unique uses in quantum devices [1–3]. Although lanthanides have been studied extensively by CW EPR, there are a few reports of pulse measurements of electron spin relaxation times, which are fundamental to the performance of some devices. In addition, most prior studies of lanthanides have been in single crystals, and it is of interest to see what information can be obtained from glassy samples. Two ions with non-Kramers $J=6$ ground states, Tb^{3+} and Tm^{3+}, were selected for comparisons, because there is little known about the relaxation times of these ions.

✉ Gareth R. Eaton
geaton@du.edu

[1] Department of Chemistry and Biochemistry, University of Denver, 2101 E. Wesley Ave, Denver, CO 80208, USA

[2] School of Pure and Applied Physics, Mahatma Gandhi University, Kottayam, India

The Tb^{3+} ion has a $4f^8$ electron configuration and $S=3$. The term with the lowest energy is ^7F with $L=3$. Strong spin–orbit coupling results in a $J=6$ ground state. The full energy-level diagram is shown in Fig. 11.1 of [4]. Tm^{3+} has a $4f^{12}$ electron configuration with $S=1$, $L=5$, and the ground state, $^3H_6$, has $J=6$. For both ions, the splitting of the M_J levels is symmetry-dependent, but for axial symmetries, $M_J=\pm 6$ is the ground state.

These 3^+ cations are non-Kramers ions, so to first approximation, one does not expect to observe EPR spectra in octahedral sites with the usual excitation mode in which B_1 is perpendicular to B_0. It is predicted that the resonance of a non-Kramers ion could be observed in the ground state when B_1 is parallel to B_0 [5–7]. EPR spectra have not been observed for these ions in cubic crystal fields. However, in lower symmetry environments, EPR spectra have been observed that are attributed to energy levels that are admixtures of $M_J=\pm 6$ [8–10]. When the ground state is a nearly degenerate pair of closely spaced singlets, with other energy levels far removed, the system can be treated as a doublet with effective $S=½$ and energy splitting δ [11–13]. The Hamiltonian is shown in Eq. (1):

$$H = g_z \beta H_z S_z + A S_z I_z + \delta S_x. \tag{1}$$

Observation of an EPR signal requires that the EPR quantum ($h\nu$) is larger than δ.

Baker and Bleaney [11] observed resonance for Tb^{3+} in sites with C_{3h} symmetry in a single crystal of yttrium ethylsulfate, and described it as an effective spin-½ system with $g_{\|}=17.7$, using the Hamiltonian in Eq. (1). Abragam and Bleaney [5] reported that no resonance had been found for Tm^{3+} in the C_{3v} site in either the chloride or the ethylsulfate salts, and that the ground state should be a singlet [5]. Moll et al. subsequently showed that EPR spectra for Tm^{3+} in Tm ethylsulfate or Tm doped into Ln ethylsulfate could be observed with high-field EPR and frequencies in the range of 1000–1600 GHz [14]. The g values depend strongly on the environment. For Tb^{3+}, $g_{\|}$ is predicted to be 17–18, and for Tm^{3+}, $g_{\|}$ is predicted to be 13.8, and $g_{\perp}$ is about 0. The g values of Tb^{3+} and Tm^{3+} ions in several environments have been reported [15–17].

2 Experiment

$La_2(oxalate)_3$ decahydrate crystals doped with Tb^{3+} were grown as previously described [18, 19]. The doping level was 2%, which corresponds to about 50 mM. Multiple crystals were placed in a 4 mm-diameter quartz tube, evacuated, back filled with He gas to about 200 mtorr, and then flame-sealed. $TbCl_3{\cdot}6H_2O$ (99.999% metals basis) and $TmCl_3{\cdot}xH_2O$ (99.99%) were purchased from Alfa Aesar for the spin-echo measurements. Because of the similarity in the CW EPR spectra that were obtained for Tb^3 and Tm^{3+} with salts of lower purity, the high purity salts were used for the relaxation measurements to ensure that the results were not due to impurities that arise from imperfect separation of the lanthanides. $TbCl_3$ or $TmCl_3$ was dissolved in 1:1 water:ethanol with pH adjusted to 2.5 with HCl. Air was removed by several freeze–pump–thaw cycles on a vacuum line and flame-sealed. For the

pulse measurements of T_1 and T_m, the sample tubes were backfilled with He gas to a pressure of about 100 mtorr prior to flame sealing. The low pressure He provides thermal contact between the sample and the walls of the tube to facilitate thermal equilibration.

CW and pulsed EPR measurements were performed on a Bruker E580 spectrometer using an ER4118XMS5 split ring resonator or an ER4118XMD5-W1 dielectric resonator in a CF935 cryostat. Temperature was controlled with a Bruker/ColdEdge Stinger closed cycle He system. An Oxford ITC503 controller was used to control heating at the bottom of the cryostat to establish the desired temperature. Sample temperature was measured with a Lakeshore Cernox sensor located near the sample, external to the resonator. The He gas flow was fast enough that the sample temperature equilibrated with the cryostat inlet temperature in less than 15 min. T_m was measured using a π/2–τ–π-echo sequence and time constants were calculated by fitting to the peaks of the modulation, using locally written software. T_1 was measured with a π-*T*–π/2-τ-π-echo inversion-recovery sequence. The instrument dead-time prevented using inter-pulse spacings of less than about 160 ns. The inversion-recovery curves were not single exponential decays, which is attributed to a distribution of relaxation times, and is common for metal ions [20]. T_1 also was measured with a picket-fence saturation recovery sequence that can be represented as $(p-d_1)_m-(d_1+dx)$ followed by two-pulse echo detection, where p is a pulse with arbitrary turning angle and dx is incremented to record the recovery curve. Most of the data for this study were acquired with p set to π/2. The delay d_1 was increased to decrease the contributions from spectral diffusion. The inversion-recovery and the picket-fence data were analyzed as the sum of two exponentials, as stretched exponentials [20, 21], and with a model-free distribution of exponentials (UPEN) [22, 23] to characterize the distributions. The numbers in the tables and in Fig. 5 were calculated from the peaks at longer times in the UPEN distributions. For the high concentration $Tb_2(oxalate)_3$ sample, the recovery curves were dominated by spectral diffusion, so T_1 estimated from the UPEN distributions is shorter than the 'true' T_1.

CW and field-stepped direct-detected spectra were acquired on a modified Bruker E500T using previously described methods [24]. This methodology is similar to 'rapid scan', but the rapid scan designation is not used in this report, because the rates of scan are slow relative to the fast relaxation rates for the lanthanides even at 4.2 K. The field-stepped direct-detected EPR method was applied to avoid the passage effects that can be observed due to magnetic field modulation when the relaxation times are too long. In addition, given the few EPR studies of Tb^{3+} and Tm^{3+} ions, we consider it important to use the new stepped-field direct-detected method in parallel with CW and pulsed EPR to demonstrate its applicability to spectra with very wide lines.

The sample for field-stepped direct-detection was in an ER4118XMD5 dielectric resonator in a substantially metal-free cryostat designed to minimize eddy currents from the rapid magnetic field scans. Temperature was controlled with the Stinger system. The temperature at the sample was measured with a calibrated Lakeshore Cernox sensor. Spin echo intensities show that signal extends beyond the magnetic field range of the direct detection measurements, and the data do not include a baseline at high field. Relative intensities of the field-stepped direct-detected spectra in

Figs. 1b and 2b were increased in scale to match the observed intensity in the echo-detected experiments.

3 Results

CW, field-stepped direct-detected, and field-swept echo-detected spectra for Tb^{3+} and Tm^{3+} in water:ethanol are shown in Figs. 1 and 2, respectively. The CW spectra of Tm^{3+} (Fig. 2) are similar to X-band spectra for Tm^{3+} in a fluorozirconate glass reported by Harris and Furniss [9], attributed to a $|M_J>= \ |\pm 6>$ ground state, and simulated with effective $S=½$ and the Hamiltonian, as shown in Eq. (1). There is considerable similarity in the spectra of Tm^{3+} and Tb^{3+} in the fluorozirconate glass.

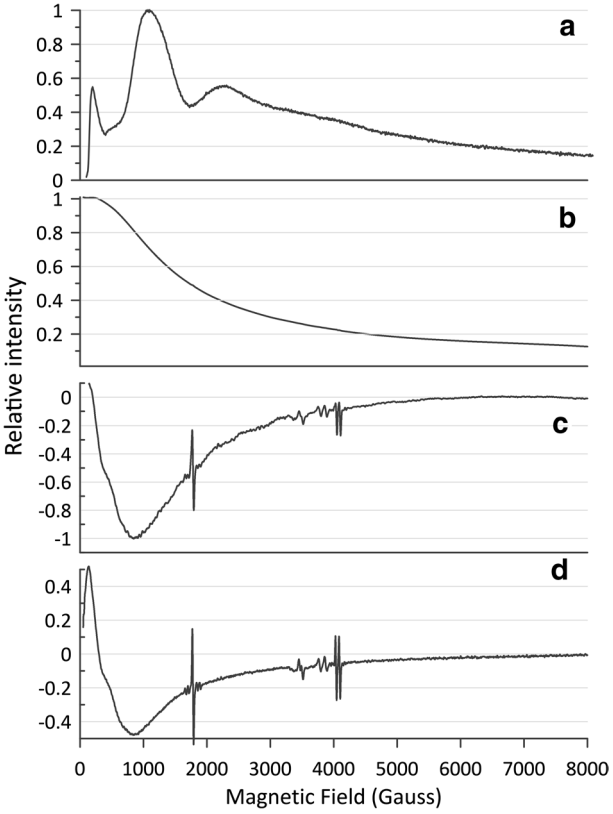

Fig. 1 Spectra of Tb^{3+} in 1:1 water:ethanol. **a** Field-swept echo-detected spectrum at 4.2 K obtained with 40 and 80 ns pulses and a constant pulse spacing of 180 ns. **b** Field-stepped direct-detected spectrum at 6 K obtained with a scan frequency of 3.6 kHz and scan segments of 25 G. **c** Derivative of the spectrum in part B. **d** CW spectrum at 5.4 K obtained with 4 G modulation amplitude at 100 kHz. Sharp signals at about 1800 G, 3500 G, and 4000 G in the CW and direct-detected spectra are from impurities in the dielectric resonator and are not observed in the pulse experiments, because the experimental parameters were not optimized for the impurity signal

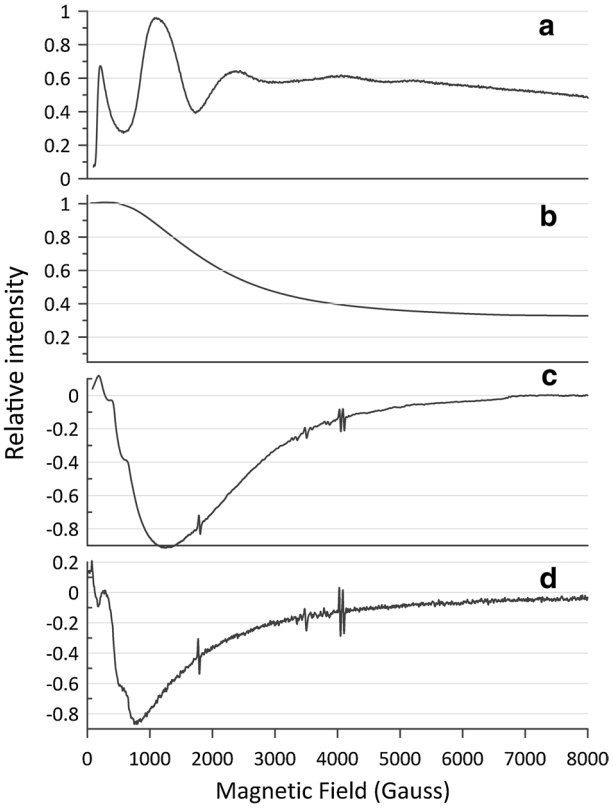

Fig. 2 Spectra of Tm^{3+} in 1:1 water:ethanol. **a** Field-swept echo-detected spectrum at 4.2 K obtained with 40 and 80 ns pulses and a constant pulse spacing of 180 ns. **b** Field-stepped direct-detected spectrum at 4.5 K obtained with a scan frequency of 3.6 kHz and scan segments of 25 G. **c** Derivative of the spectrum in part B. **d** CW spectrum at 4.5 K obtained with 4 G modulation amplitude at 100 kHz. Sharp signals at about 1800 G, 3500 G, and 4000 G in the CW and direct-detected spectra are from impurities in the dielectric resonator and are not observed in the pulse experiments, because the experimental parameters were not optimized for the impurity signal

The field-swept echo-detected spectra sometimes had an artifact near zero-field because of limitations in the mechanical sweep of the magnet power supply of the E580 system. The shape of the field-swept echo-detected spectra depends on the time between the two pulses used to create the echo. In two-pulse echo decays, echo envelope modulation from protons in the solvent is very deep at low magnetic fields (Fig. 3). Since the period for the modulation varies with field, the time for the maxima in the modulation varies with field, which causes variation in the intensity of the echo at constant spacing between the two pulses. This variation is conspicuous in the field-swept echo-detected spectra for both Tm^{3+} and Tb^{3+} at fields below about 3000 G. The combined information from the three detection modalities is that the EPR signals for these ions extend from almost zero field to relatively high field, consistent with large g anisotropy, and are similar for Tb^{3+} and Tm^{3+}. Both

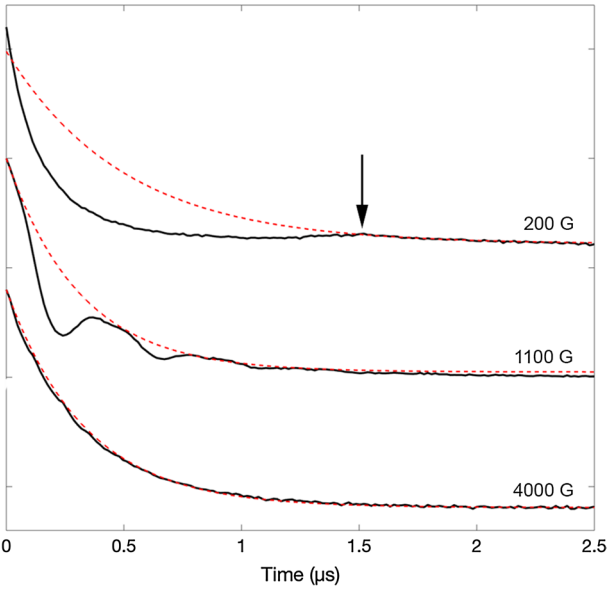

Fig. 3 Field dependence of two-pulse spin-echo decay curves for 10 mM Tm^{3+} in 1:1 water:ethanol at 4.2 K at 200 G, 1100 G, and 4000 G. The red-dashed lines are single exponential fits to the data, shown in black. Data recorded at 200 and 1100 G were fit to a single exponential by selecting the maximum of the modulation peaks present using T_m of 0.25 and 0.17 μs at 200 and 1100 G, respectively. Data recorded at 4000 G was fit to a single exponential model without peak-picking using a T_m of 0.33 μs (colour figure online)

the field-swept echo-detected spectra and the field-stepped direct-detected spectra highlight the fact that there is substantial signal intensity extending beyond 8000 G. This fact is less obvious in the CW spectra and in the first-derivative of the field-stepped direct-detected spectra, because the slope of the absorption signal is small at high field. These results are consistent with the prediction of $g_{\perp} \sim 0$. The field-swept echo-detected spectra for $Tb_2(oxalate)_3$ in $La_2(oxalate)_3$ are similar to the spectrum shown in Fig. 1a for Tb^{3+} in water:ethanol. In the $La_2(oxalate)_3$ decahydrate crystal, the Tb^{3+} presumably is coordinated by nine oxygen atoms [25], possibly with some distortion, because the Tb^{3+} is smaller than La^{3+}. The coordination environment may have similar symmetry (or lack thereof) in the glassy frozen water:ethanol, so it is not surprising that the EPR spectra are similar in the crystal and in the frozen solution.

3.1 Pulse Turning Angles

Although the spectrometer is equipped with a 1 kW TWT amplifier, very low excitation powers are needed for π/2 pulses, because $J = 6$ and the g value is large. The degree of over-coupling of the resonator that was used for the pulse experiments would normally require about 6–10 dB attenuation of the TWT output for a spin-½ at $g \approx 2$, using 40 ns π/2 pulses. For the Tb^{3+}-doped $La_2(oxalate)_3$ sample, the echo

maximum was at about 27 dB attenuation. The Tb^{3+} and Tm^{3+} water:ethanol solutions required about 18–23 dB attenuation, depending on the degree of over-coupling [26].

Turning angles for various spins S at the same B_1 depend on the raising and lowering operator. Less incident microwave power is required to produce a π/2 pulse for larger S. Note that this is true for high-spin systems even if the transition being observed is $m_S = +½ \leftrightarrow -½$. To include the dependence on S, the flip angle equation, Θ, can be written as:

$$\Theta = c\gamma B_1 t_p \text{ where } c = \left[S(S+1) = m_S\left(m_S+1\right)\right]^{1/2} \quad (2)$$

for the transition between m_s and $m_s + 1$ for a system with spin S.

For Tb^{3+} and Tm^{3+} with strong spin–orbit coupling that is typical for lanthanides, J is a good quantum number, so it is used in Eq. (2) in place of S. Substitution of $J = 6$ and $m_J = -½$ into Eq. (2) gives c for these samples that is 6.5 times larger than for $S = ½$. Since B_1 is proportional to the square root of power, this increase in c predicts that about $(6.5)^2 = \sim 42$ times less incident power is required to achieve a π/2 pulse for a $J = 6$ spin system than is required for an $S = ½$ spin system. This prediction is consistent, within the reproducibility of over-coupling, with the ~ 16 dB (factor of 40) larger attenuation levels used for the lanthanides than for $S = ½$ systems in the same resonator.

The shape of a field-swept echo-detected EPR spectrum depends on the B_1 of the pulse, the separation between the pulses, and the portion of the echo that is detected. The pulses excite only a very small portion of the spectrum, so relaxation times may include spectral diffusion in addition to longitudinal and transverse relaxation processes. Checks of the effects of B_1 and pulse length did not reveal evidence of instantaneous diffusion or spectral diffusion in the 2-pulse echo for the water:ethanol solutions.

3.2 Relaxation Times

Examples of spin-echo decays as a function of position in the spectrum at 4.2 K are shown in Fig. 3. At 200 G, the proton echo envelope modulation is so deep that there is only a single low intensity peak of the first modulation cycle, which might not have been detected if the signal-to-noise were poorer. Modulation depth decreases with increasing field, consistent with theory [27].

A comparison of T_1 obtained by inversion-recovery and picket-fence saturation recovery experiments is shown in Fig. 4. The inversion-recovery data (Fig. 4a) can be fit well with a stretched exponential of 16.3 μs and an exponent of 0.63 or as the sum of two exponentials with time constants of 24 and 4 μs. The UPEN analysis of the inversion-recovery curve shows a broad distribution of relaxation times (Fig. 4d). The value at the peak in the distribution at long relaxation times is similar to, though less well defined than, the value obtained in the picket-fence saturation experiments (Fig. 4e, f). Standard 3-pulse echo measurements of T_1 may include contributions from spectral diffusion, T_{SD}, as well as T_1, if the spectral diffusion is neither very fast or very slow relative to T_1 [28–30]. Consequently, it is reasonable

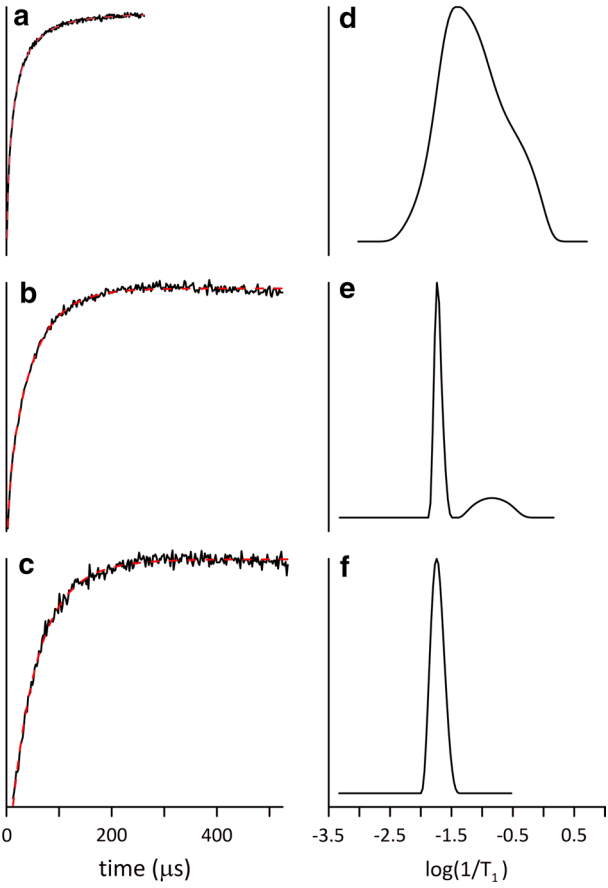

Fig. 4 Measurements of T_1 for Tb^{3+}in 1:1 water:ethanol at 5 K obtained by **a** inversion recovery, **b** picket-fence saturation recovery with 2 μs spacing of the pickets, **c** picket-fence saturation recovery with 12 μs spacing of the pickets, and the corresponding distributions of relaxation rates in 1/μs obtained with UPEN shown in **d**–**f**. The fits to the recovery curves using the parameters obtained with UPEN are shown with red-dashed lines

to attribute the faster-relaxing components of the inversion-recovery results to spectral diffusion. Because of the very large g anisotropy and unresolved nuclear coupling in the spectra of Tb^{3+} and Tm^{3+}, spectral diffusion is a reasonable expectation. As discussed below, long-pulse saturation recovery, the usual way to separate T_{SD} from T_1, is not practical for Tb^{3+} and Tm^{3+}. A close approximation can be achieved with the picket-fence multiple-pulse saturation of spectral diffusion, followed by two-pulse echo-detected recovery. A method of saturating a resonance with a series of short pulses (a 'saturating comb') and then monitoring the magnitude of M_z with an FID was reported in the NMR review by Narath [31]. This 'picket' method was adopted in EPR with spin-echo monitor of M_z by Dalton et al. [32]. Guidance on performance of the picket method was presented by Bowman [33]. In this method,

many pulses are used to drive magnetization away from the z-axis, equilibrating any spectral diffusion in the excited spin packets during the pulse sequence. The Bruker Xepr PulseSPEL software on the E580 permits a sequence of up to 30 pulses of arbitrary length and with a wide range of times between pulses. UPEN analysis of data from a picket-fence measurement with 30 picket-pulses and a 2 μs pulse spacing (Fig. 4b) has a well-defined T_1 of 56 μs and a small contribution from a faster process that is attributed to spectral diffusion (Fig. 4e. Analysis of this data set as the sum of two exponentials gives a long component with time constant of 51 μs. Fitting with a stretched exponential gives a time constant of 48 μs, which is approaching the UPEN value, and an exponent of 0.94 which is approaching 1 consistent with narrowing of the distribution. When the pulse spacing was increased to 12 μs (Fig. 4c), the most probable T_1 is 55 μs and there is negligible contribution from spectral diffusion. Fitting of these data as the sum of two exponentials gives a long time constant of 56 μs, demonstrating that analysis of the picket-fence recovery curves as the sum of two exponentials gives a time constant for the long component that is in good agreement with the results from the UPEN analysis. Fitting these data with a stretched exponential gives $T_1 = 53$ μs and an exponent of 0.99, consistent with a relatively narrow distribution. The UPEN analysis has the advantage that the contributions from multiple components can be visualized [20]. We conclude that the picket-fence saturation recovery measurements at 5 K permit separation of the contributions to the experimental recovery curves and support the assignment of the faster components as spectral diffusion.

The temperature dependence of relaxation rates for Tb^{3+} and Tm^{3+} in water:ethanol is shown in Fig. 5. The time-domain data were too weak and

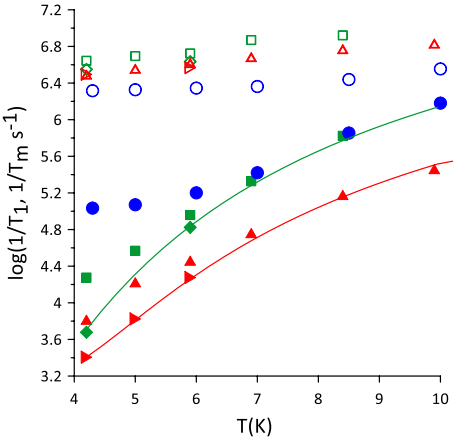

Fig. 5 Temperature dependence of relaxation rates. $1/T_m$ for (green square) 10 mM Tb^{3+} in 1:1 water:ethanol, (green diamond) 1 mM Tb^{3+} in 1:1 water:ethanol, (blue circle) $Tb_2(oxalate)_3$ in $La(oxalate)_3$, (red triangle) 10 mM Tm^{3+} in 1:1 water:ethanol, (red horizontal triangle) 1 mM Tm^{3+} in 1:1 water:ethanol; $1/T_1$ for (green filled triangle) 10 mM Tb^{3+} in 1:1 water:ethanol, (green filled diamond) 1 mM Tb^{3+} in 1:1 water:ethanol, (blue filled circle) $Tb_2(oxalate)_3$ in $La(oxalate)_3$, (red filled triangle) 10 mM Tm^{3+} in 1:1 water:ethanol, and (red horizontal triangle) 1 mM Tm^{3+} in 1:1 water:ethanol. The solid lines are fits to the temperature dependence of $1/T_1$ including contributions from the direct and Raman processes

relaxation rates too fast to obtain reliable relaxation times above ca. 10 K. T_1 for Tb^{3+} and Tm^{3+} in water:ethanol are shown for 1100 G, which is the maximum in the field-swept echo-detected spectrum. Values of T_1 for $Tb_2(oxalate)_3$ in $La_2(oxalate)_3$ crystals are reported for 650 G. Spin–lattice relaxation rates are consistently faster for Tb^{3+} than for Tm^{3+}. For both ions, the relaxation rates increase rapidly with increasing temperature with about a T^4 dependence. At temperatures between 4.2 and 6 K, T_1 is concentration-dependent. The shorter T_1 for the 10 mM solutions than for the 1 mM solutions demonstrates that metal–metal dipolar interactions and cross relaxation dominate relaxation at the higher concentration. This might seem surprising for a spectrum that extends over the entire accessible magnetic field range at X-band, such that the spins/gauss is small, but the magnetic moments are large. For the high concentration $Tb_2(oxalate)_3$ in $La_2(oxalate)_3$ crystal $1/T_1$ is weakly temperature-dependent between about 4 and 6 K, which is characteristic of samples with very high-spin concentrations. The high concentration (~ 50 mM) results in cross relaxation that makes $1/T_1$ faster in the crystal near 4 K.

The temperature dependence of $1/T_1$ was modeled using Eq. (2) [34]:

$$\frac{1}{T_1} = A_{\mathrm{dir}}T + A_{\mathrm{Ram}}\left(\frac{T}{\theta_D}\right)^9 J_8\left(\frac{\theta_D}{T}\right) + A_{\mathrm{orb}}\left[\frac{\Delta_{\mathrm{orb}}^3}{\mathrm{e}^{\Delta_{\mathrm{orb}}/T}-1}\right], \tag{2}$$

where A_{dir} is an experimentally determined adjustable parameter, T is temperature, A_{Ram} is an experimentally determined adjustable parameter that scales the contribution from the two-photon Raman process [35, 36], and J_8 is the transport integral Eq. (3), that was developed to model heat capacity, A_{orb} is an experimentally determined adjustable parameter that scales the contribution from the Orbach process, and Δ_{orb} is the energy of the low-lying excited state for the Orbach process [37]:

$$J_8\left(\frac{\theta_D}{T}\right) = \int_0^{\theta_D/T} x^8 \frac{\mathrm{e}^x}{(\mathrm{e}^x-1)^2}\mathrm{d}x \tag{3}$$

Above about 6 K, the echoes for the 1 mM samples were too weak to acquire data with acceptable signal-to-noise, so the modeling was based on T_1 for 1 mM samples at 4.2 to 6 K and for 10 mM samples at 6.9–9.9 K. The concentration dependence of T_1 between 1 and 10 mM at 4 to 6 K is evidence for a substantial contribution from cross relaxation at the lowest temperatures and higher concentrations, which has the same temperature dependence as the direct process. The strong temperature dependence of T_1 is characteristic of the Raman process at temperatures well below the Debye temperature. The fits to the experimental data shown in Fig. 5 were calculated as the sum of contributions from the direct process and the Raman process. A small contribution from an Orbach process cannot be ruled out, but this process predicts a weaker temperature dependence, so it cannot be the dominant contribution. The fit parameters for Tm^{3+} are $A_{\mathrm{dir}} = 320\ \mathrm{s}^{-1}$, Debye temperature = 54 K, and $A_{\mathrm{Ram}} = 3.2\times10^8\ \mathrm{s}^{-1}\ \mathrm{K}^{-1}$. For Tb^{3+} $A_{\mathrm{dir}} = 0\ \mathrm{s}^{-1}\ \mathrm{K}^{-1}$, Debye temperature = 54 K, and $A_{\mathrm{Ram}} = 1.4\times10^9\ \mathrm{s}^{-1}\ \mathrm{K}^{-1}$.

Table 1 T_1 (μs) in 1:1 water:ethanol at 4.2 K

Field (G)	200	1100	4000
Tb^{3+}	45	53	42
Tm^{3+}	118	159	125

For 10 mM solutions. Data were fit with UPEN. The values shown are the peaks in the distribution at long relaxation times. Uncertainties are about 20%

Table 2 Relaxation times for $Tb_2(oxalate)_3$ at 4.2–4.3 K

Field (G)	220	650	800	950	2000
T_1 (μs)	11	15	14	22	22
T_m (ns)	0.31	0.33	0.36	0.35	0.44

Values of T_1 were estimated from the peaks in UPEN distributions at long relaxation times. Uncertainties are about 25% for T_1 and 10% for T_m

T_1 is weakly dependent on the position in the spectrum as listed in Table 1 for the 10 mM solutions at 4.2 K and in Table 2 for the $Tb_2(oxalate)_3$ in $La_2(oxalate)_3$ at 4.3 K. These T_1 values in the μs range at 4.2 K are orders of magnitude shorter than for typical transition metals [30, 38, 39]. Matrix elements for transitions between states of non-Kramers ions are non-zero, making modulation of spin–orbit coupling by vibrations more effective, and thereby making relaxation times shorter [40]:

The Tb^{3+} ions in the doped $La_2(oxalate)_3$ decahydrate crystal and in the water:ethanol solutions exhibit strong ^1H modulation in the spin-echo measurements at the low magnetic fields that correspond to the large $g_{\|}$ values (Fig. 3). Deep modulation at low fields adds uncertainty to values of T_m. The T_m values plotted for the water:ethanol samples (Fig. 5) were measured at 4000 G, where nuclear modulation was not observed and single exponentials fit the data well (Fig. 2). T_m values for Tb^{3+} in $La_2(oxalate)_3$ crystals are reported for 650 G, although there is substantial echo modulation. Values of T_m for the 10 mM 1:1 water ethanol solutions are similar for Tm^{3+} and Tb^{3+} and much shorter than the ~ 4 μs that is typical for organic radicals and transition metals in organic solvents at 4.2 K [30]. At these low temperatures, phase memory dephasing for organic radicals and 3d transition metals is attributed to nuclear spin diffusion that modulates the electron–proton dipolar interaction [41, 42]. The large spins of the Tb^{3+} and Tm^{3+} ions increase the dipolar interaction which makes the nuclear spin diffusion a more effective dephasing mechanism and shortens T_m. The proton spin concentration in the oxalate salt is lower than in 1:1 water:ethanol, so T_m is longer for the terbium oxalate crystal, in spite of the higher electron spin concentration. Because of the large g anisotropy, even very small motion takes the spin off resonance and may provide additional explanation for the very short values of T_m. For the $Tb_2(oxalate)_3$ crystals, there was a trend toward shorter T_m (493–422 ns) as the π/2 pulse was increased from 16 to 160 ns, suggesting significant spectral diffusion.

4 Discussion

CW EPR of integer-spin species usually yields stronger signals when obtained in parallel mode (B_1|| to B_0) rather than in the usual perpendicular mode ($B_1\perp$ to B_0). Thus, it might be a surprise that normal perpendicular mode B_1 was used in the CW, pulse, and direct-detected spectra reported in this paper. Abragam and Bleaney [5] report that EPR of these ions is observed in parallel mode, and explain the $g_{||}=17.72$ as due to mixing of the state $|M_J>=|0>$ with $|M_J>=|\pm 6>$. Relaxation in zero magnetic field was measured by Larsen and Jeffries [43]. The spin selection rule is $\Delta M_J=\pm 1$. The g value depends strongly on the symmetry of the environment of the Tb^{3+} ion in doped solids. The values for $g_{||}$ range from ca. 17.8–10.44 and 4.66 in sites of C_{3v} symmetry [17]. The samples studied in this paper are consistent with the larger g value reported previously.

As several cited papers, and Abragam and Bleaney [5], explain, since $4f^{12}$ Tm^{3+} is a non-Kramers ion with $^3H_6$ multiplet, one does not expect to have doublet ground states and, hence, EPR spectra are not expected. However, it has been shown that mixing excited states into the ground state makes transitions in the ground state allowed [5, 44]. If the degeneracies are removed by the environment of the ion, only singlet states will occur. However, if some degeneracy remains, then the ion can have an effective $S=½$ state. The same argument applies to the $4f^8$ Tb^{3+} $^7F_6$ ion. Baker et al. [8] stated that the spectra observed in lanthanum nicotinate dihydrate could not be attributed to isolated Tm^{3+} ions, but instead are from pairs of Tm^{3+}. They show good agreement between line intensities for Tm^{3+} in lanthanum nicotinate dihydrate and predictions that the intensities should be proportional to the square of the matrix elements of $g_z\mu_B B_{1z}(S_{1z}+S_{2z})$. These transitions involve B_1 parallel to the magnetic field. Baker et al. describe the Tb^{3+} analog as exhibiting "properties as strange as those of Tm^{3+}" [45].

4.1 Comparison with Prior Work

The books by Abragam and Bleaney [46], Orton [6], and Standley and Vaughan [39], and the 1994 review by Bertini et al. [38] provide comprehensive reviews of the literature up to their publication dates. There is precedent for observing EPR of the non-Kramers ions, and for measuring relaxation times in some lattice environments. Field-swept echo-detected spectra of Ce^{3+}, Nd^{3+}, Er^{3+}, and Yb^{3+} ions dissolved in water:glycerol and in water:ethanol were reported by Mims and Davis [47], but we have not found reports of Tb^{3+} or Tm^{3+} dissolved in these solvents.

Tm^{3+} EPR signals were observed in single crystals of thulium ethylsulfate [48]. Previously, EPR had not been observed for Tm^{3+} diluted in yttrium ethylsulfate. The signals were attributed to Tm^{3+} at sites of C_{2v} or lower symmetry.

The description of Tb^{3+} as "characterized by narrow resonance lines" [49] apparently refers to the CW X-band transition near 600 G, which, under certain incident power conditions, can look like a narrow line. However, the spectra extend over more than 12,000 G in both CW and pulsed EPR, with about 40% of the maximum intensity still present at 12,000 G in pulsed EPR spectra. Because of the long

relaxation times at 4.2 K, the CW spectra depend strongly on incident microwave power and modulation frequency and amplitude.

Other reports of CW spectra in various crystal environments include for Tb^{3+} [16, 17, 45, 50, 51] and for Tm^{3+} [1, 2, 8, 10, 16, 40, 44, 52–57].

No prior measurements of T_m have been found for Tb^{3+}. The only prior measurements of T_m for Tm^{3+} are by Solovarov and coworkers [1] and Sukhanov and coworkers [40]. Tm^{3+} in synthetic Forsterite exhibited $T_m = 500$ ns with B_1 parallel to the magnetic field at 4.2 K [1]. Relaxation of Tm^{3+} in Y_2SiO_5 was measured by pulse methods at W-band (94 GHz) from 5 to 15 K [40]. A Carr–Purcell–Meiboom–Gill sequence gave longer T_m than did the two-pulse Hahn echo decay, and T_m was concentration dependent. The host lattice contained ^{28}Si, to decrease the nuclear spin concentration. For the 0.001% Tm^{3+} sample, T_m was about 10 μs at 7–12 K. The relatively long value of T_m is attributed to the combined effect of the low concentration of nuclear spins which decreases nuclear spin–spin diffusion and the low concentration of paramagnetic species which decreases electron–electron dipolar interaction. T_1 was about 90 μs at 5 K and decreased to about 10 μs at 15 K, which is a dependence of ca. $T^{8.2}$ [40] that can arise from the Raman process. The splitting between the ground state and the first excited singlet electronic level was found to be 50.6 GHz. An echo-detected spectrum of Tb^{3+} was measured at 1.5 K and 94 GHz with inter-pulse spacing of 400 ns [58].

Prior work generally found shorter T_1 with increasing lanthanide spin concentration, especially near 4 K [59]. Our observations of concentration dependence (Fig. 5) are consistent with that pattern. Consequently, the T_1 values reported here are not the low-concentration limit, nor are they free of spectral diffusion contributions. T_1 of Tb^{3+} and Tm^{3+} depends on the crystal environment, spin concentration, microwave frequency, and magnetic field, in addition to temperature. Several studies observed T_1 at X-band near 4 K similar to the values reported here [60–63]. Several relaxation measurements of Tb^{3+} in various solids at X-band were tabulated by Standley and Vaughan [39]. A direct process and T^7 dependence were observed in the helium temperature range.

4.2 Difficulties in EPR of Lanthanides in Powders or Glasses

Lanthanides with spectra over the entire accessible magnetic field range pose an extreme challenge. There is no baseline data; no place at which the EPR signal is zero. Regions without signal are normally relied upon to define baseline corrections for CW spectra and phasing of direct-detected spectra. The presence of signal at high field could easily be missed in the first-derivative CW spectra, because a slowly changing intensity has near-zero derivative, which can incorrectly be interpreted as a region of no EPR transitions. Relaxation time measurements of lanthanides also present challenges. Spin echo measurements can provide T_m by two-pulse echo decay, and an estimate of T_1 by inversion recovery, but both measurements may be dominated by spectral diffusion. Saturation recovery spectra are a special problem, because they almost always require subtraction of off-resonance signals. In these Tm^{3+} and Tb^{3+} data where EPR intensity is present at all accessible fields, there is

no way to subtract out instrumental artifacts. If the EPR signal is known to be much more intense than instrumental artifacts, the pulse method results may be a good approximation to the relaxation times. Some spectral diffusion can be obviated by pulse methods that suppress the effects of diffusion, such as the "picket fence" of repetitive preparation pulses that approximate long-pulse saturation recovery. No literature reports have been found that discuss this problem.

4.3 Signal Quantitation

Determining the absolute intensity of CW or pulsed EPR is difficult, but with good characterization of the resonator B_1 and modulation field distributions, it has been demonstrated that EPR spectra can be quantitatively compared with good precision and accuracy [64]. Inherent in these quantitative measurements, however, is the often unstated assumption that there is well-defined baseline on the low-field and high-field extremes of the spectra. For many of the X-band lanthanide powder spectra, there is intensity over all accessible magnetic fields—roughly 0–13,000 G on a standard commercial magnet, and beyond. It is almost impossible to have a well-defined, linear, baseline over the full magnetic field range of the spectrometer. Consequently, it is not possible to define the integral of the lanthanide spectra. However, each of the lanthanides is available in very high purity—99.99 or 99.999%—so one can make quantitative standards with whatever environment is appropriate for comparisons with samples of unknown concentration, and measure the intensity at a defined field, rather than an integral over the full spectrum. This is a general problem for any spectrum that extends beyond the magnetic field range of the spectrometer used, and not limited to lanthanides.

4.4 Spectral Diffusion

Processes that take spins off resonance on the timescale of the pulse experiments are designated as spectral diffusion [30]. This may include motion which is concentration independent, cross relaxation which depends on the concentration of the paramagnetic species, and mutual flips of nuclear spins in the environment which depends on the concentration of the nuclear spins. For the samples studied here, the spectral diffusion contribution is substantially greater for the higher concentration samples.

5 Summary

First derivative, magnetic-field-modulated EPR spectra of Tb^{3+} or Tm^{3+} have the appearance of a peak at low magnetic field due to the high $g_{\|}$ value. Slowly changing amplitude as a function of magnetic field results in near-zero slope at higher field. The CW signal saturates and displays passage effects readily near 4.2 K and becomes weak and difficult to observe near 10 K. The phase memory time is very short, which we attribute to the very large change in field that occurs due to very

small angular motions of the ion and to the enhanced effectiveness of nuclear spin diffusion because of the large spins of the paramagnetic ions and resulting increase in dipolar interactions. Field-swept echo-detected spectra exhibit considerable structure and are not simply analogs of the integral of the CW spectra, due to nuclear modulation and field dependence of T_m. Pulse spectra show strong signals where the CW spectrum looks negligible, because the slope is near zero. Field-stepped direct-detected spectra combine important features selected by CW and pulsed spectra. T_1 depends strongly on temperature.

Acknowledgements This research was partially funded by NIH NCI R01 CA 177744. The closed cycle cooling system was developed by ColdEdge Technologies, Allentown PA, and installed with assistance by Dr. Arthur H. Heiss. Dr. Velavan Kathirvelu, National Institute of Technology Goa, assisted in providing the Tb^{3+} in $La_2(oxalate)_3$ crystals.

References

1. N.K. Solovarov, V.F. Tarasov, E.V. Zharikov, JETP Lett. **104**, 94–98 (2016)
2. V.F. Tarasov, N.K. Solovarov, E.V. Zharikov, Opt. Spectrosc. **121**, 560–566 (2016)
3. D. Parker, E.A. Suturina, I. Kuprov, N.F. Chilton, Acc. Chem. Res. **53**, 1520–1534 (2020)
4. A.E. Merbach, E. Toth, *The Chemistry of Contrast Agents in Magnetic Resonance Imaging* (Wiley, Chichester, 2001)
5. A. Abragam, B. Bleaney, *Electron Paramagnetic Resonance of Transition Ions* (Oxford University Press, Oxford, 1970), pp. 302–320
6. J.W. Orton, *Electron Paramagnetic Resonance: An Introduction to Transition Group Ions in Crystals* (Gordon and Breach, New York, 1968)
7. A. Schweiger, G. Jeschke, *Principles of Pulse Electron Paramagnetic Resonance* (Oxford University Press, Oxford, 2001), p. 58 and 263
8. J.M. Baker, J.C.A. Hutchison, P.M. Martineau, Proc. R. Soc. Lond. A Math. Phys. Sci. **403**, 221–233 (1986)
9. E.A. Harris, D. Furniss, J. Phys. C Solid State Phys. **21**, 7–15 (1988)
10. V.A. Pashchenko, A.G.M. Jansen, M.I. Kobets, E.N. Khats'ko, P. Wyder, Phys. Rev. B **62**, 1197–1202 (2000)
11. J.M. Baker, B. Bleaney, Proc. Phys. Soc. A **68**, 257 (1955)
12. J.S. Griffith, Phys. Rev. **132**, 316–319 (1963)
13. G. Jeschke, A. Schweiger, J. Chem. Phys. **106**, 9979–9991 (1997)
14. H.P. Moll, J. vanTol, P. Wyder, M.S. Tagirov, D.A. Tayurskii, Phys. Rev. Lett. **77**, 3459–3462 (1996)
15. M.J. Weber, R.W. Bierig, Phys. Rev. **134**, A1492–A1503 (1964)
16. I.N. Kurkin, E.A. Tsvetkov, Phys. Stat. Solid A **25**, 731–737 (1974)
17. J.W. Jewett, P.E. Wigen, J. Chem. Phys. **61**, 2991–2995 (1974)
18. M.C. Minu, G. Vimal, K.P. Mani, G. Jose, P.R. Biju, C. Joseph, N.V. Unnikrishnan, M.A. Ittyachen, J. Mater. Res. Technol. **5**, 268–274 (2016)
19. G. Vimal, K.P. Mani, G. Jose, P.R. Biju, C. Joseph, N.V. Unnikrishnan, M.A. Ittyachen, J. Cryst. Growth **404**, 20–25 (2014)
20. T. Ngendahimana, R. Ayikpoe, J.A. Latham, G.R. Eaton, S.S. Eaton, J. Inorg. Biochem. (2019). https://doi.org/10.1016/j.jinorgbio.2019.110806
21. M. Laviolette, M. Auger, S. Desilets, Macromolecules **32**, 1602–1610 (1999)
22. G.C. Borgia, R.J.S. Brown, P. Fantazzini, J. Magn. Reson. **132**, 65–77 (1998)
23. G.C. Borgia, R.J.S. Brown, P. Fantazzini, J. Magn. Reson. **147**, 273–285 (2000)
24. Z. Yu, T. Liu, H. Elajaili, G.A. Rinard, S.S. Eaton, G.R. Eaton, J. Magn. Reson. **258**, 58–64 (2015)
25. S.-H. Huang, G.-D. Zhou, T.C.W. Mak, J. Cryst. Spectrosc. Res. **21**, 127–131 (1991)
26. G.A. Rinard, R.W. Quine, S.S. Eaton, G.R. Eaton, W. Froncisz, J. Magn. Reson. A **108**, 71–81 (1994)
27. L. Kevan, in *Time Domain Electron Spin Resonance*, ed. by L. Kevan, R.N. Schwartz (Wiley, New York, 1979), pp. 279–341
28. J.R. Harbridge, G.R. Eaton, S.S. Eaton, in *Modern applications of EPR/ESR: from biophysics to materials science. Proceedings of the Asia-Pacific EPR/ESR symposium*, 1st, Kowloon, Hong Kong, Jan 20–24, 1997, pp. 220–225 (1998)

29. J.R. Harbridge, S.S. Eaton, G.R. Eaton, J. Phys. Chem. A **107**, 598–610 (2003)
30. S.S. Eaton, G.R. Eaton, Biol. Magn. Reson. **19**, 29–154 (2000)
31. A. Narath, in *Hyperfine Interactions*, ed. by A.J. Freeman, R.B. Frankel (Academic Press, New York, 1967), p. 297
32. L.R. Dalton, A.L. Kwiram, J.A. Cowen, Chem. Phys. Lett. **14**, 77–81 (1972)
33. M.K. Bowman, in *Electron Paramagnetic Resonance: A Practitioner's Toolkit*, ed. by M. Brustolon, E. Giamello (Wiley, Hoboken, 2009), p. 174
34. S.S. Eaton, G.R. Eaton, in *Handbook of EPR Spectroscopy: Fundamentals and Methods*, ed. by D. Goldfarb, S. Stoll (Wiley, Chichester, 2018), pp. 175–192
35. A. Abragam, *The Principles of Nuclear Magnetism* (Oxford University Press, London, 1961), pp. 405–409
36. J. Murphy, Phys. Rev. **145**, 241–247 (1966)
37. J.G. Castle Jr., D.W. Feldman, Phys. Rev. A **137**, 671–673 (1965)
38. I. Bertini, G. Martini, C. Luchinat, in *Handbook of Electron Spin Resonance: Data Sources, Computer Technology, Relaxation, and ENDOR*, ed. by C.P. Poole, Jr, H.A. Farach (American Institute of Physics, New York, 1994), pp. 79–310
39. K.J. Standley, R.A. Vaughan, *Electron Spin Relaxation Phenomena in Solids* (Plenum Press, New York, 1969)
40. A.A. Sukhanov, V.F. Tarasov, Y.D. Zavartsev, A.I. Zagumennyi, S.A. Kutovoi, JETP Lett. **108**, 210–214 (2018)
41. A. Zecevic, G.R. Eaton, S.S. Eaton, M. Lindgren, Mol. Phys. **95**, 1255–1263 (1998)
42. K.M. Salikhov, Y.D. Tsvetkov, in *Time Domain Electron Spin Resonance*, ed. by L. Kevan, R.N. Schwartz (Wiley, New York, 1979), pp. 232–277
43. G.H. Larson, C.D. Jeffries, Phys. Rev. **145**, 311–324 (1966)
44. J.T. Yu, J. Phys. Chem. Solids **37**, 301–303 (1976)
45. J.M. Baker, J.C.A. Hutchison, M.J.M. Leask, P.M. Martineau, M.G. Robinson, Proc. R. Soc. Lond. A Math. Phys. Sci. **413**, 515–528 (1987)
46. A. Abragam, B. Bleaney, *Electron paramagnetic resonance of transition ions* (Oxford University Press, Oxford, 1970)
47. W.B. Mims, J.L. Davis, J. Chem. Phys. **65**, 3266–3274 (1976)
48. D.C. Baker, H.H. Dearman, J. Chem. Phys. **56**, 3664–3671 (1972)
49. M.R. Gafurov, V.A. Ivanshin, I.N. Kurkin, M.P. Rodionova, H. Keller, M. Gutmann, U. Staub, J. Magn. Reson. **161**, 210–214 (2003)
50. C.A. Hutchison, E. Wong, J. Chem. Phys. **29**, 754–760 (1958)
51. I. Laursen, L.M. Holmes, J. Phys. C Solid State Phys. **7**, 3765–3769 (1974)
52. J.B. Gruber, E.A. Karlow, D.N. Olsen, U. Ranon, Phys. Rev. B **2**, 49–53 (1970)
53. I.E. Rouse, J.B. Gruber, Phys. Rev. B **13**, 3764–3773 (1976)
54. G.R. Asatryan, A.P. Skvortsov, G.S. Shakurov, Phys. Solid State **55**, 1039–1042 (2013)
55. A.A. Konovalov, D.A. Lis, K.A. Subbotin, V.F. Tarasov, E.V. Zharikov, Appl. Magn. Reson. **30**, 673–682 (2006)
56. A.E. Nikiforov, A.Y. Zakharov, M.Y. Ugryumov, S.A. Kazanskii, A.I. Ryskin, G.S. Shakurov, Phys. Solid State **47**, 1431–1435 (2005)
57. G.S. Shakurov, V.F. Tarasov, B.Z. Malkin, A.I. Iskhakova, L.A. Kasatkina, J. Heber, M. Altwein, Appl. Magn. Reson. **14**, 415–426 (1998)
58. E.V. Edinach, Y.A. Uspenskaya, A.S. Gurin, R.A. Babunts, H.R. Asatyan, N.G. Romanov, A.G. Badalyan, P.G. Baranov, Phys. Rev. B **100**, 104435 (2019)
59. L. Rimai, R.W. Bierig, B.D. Silverman, Phys. Rev. **146**, 222–232 (1966)
60. R.W. Bierig, M.J. Weber, S.I. Warshaw, Phys. Rev. **134**, A1504–A1516 (1964)
61. B.G. Berulava, T.I. Sanadze, O.G. Khakhanashvili, Sov. Phys. Solid State **7**, 509–510 (1965)
62. R.C. Mikkelson, H.J. Stapleton, Phys. Rev. **140**, A1968–A1982 (1965)
63. G.H. Larson, C.D. Jeffries, Phys. Rev. **141**, 461–468 (1966)
64. G.R. Eaton, S.S. Eaton, D.P. Barr, R.T. Weber, *Quantitative EPR* (Springer, New York, 2010)